



ChemComm

Self-Regenerative Noble Metal Catalysts Supported on High-Entropy Oxides

Journal:	<i>ChemComm</i>
Manuscript ID	CC-COM-08-2020-005860.R1
Article Type:	Communication

SCHOLARONE™
Manuscripts

COMMUNICATION

Self-Regenerative Noble Metal Catalysts Supported on High-Entropy Oxides

Page Received 00th January 20xx,
Accepted 00th January 20xx

Hao Chen,^a Yifan Sun,^{*b} Shize Yang,^{†c} Hui Wang,^d Wojciech Dmowski,^d Takeshi Egami,^{def} Sheng Dai^{*ab}

DOI: 10.1039/x0xx00000x

Discovery of anti-sintering noble metal catalysts is challenging, as supported noble metal species tend to aggregate at high temperatures, leading to severely deteriorated catalytic performances. Here we show that 1 wt% of noble metal species including Au, Pd and Ru can be incorporated into high-entropy oxides (HEOs) through entropy stabilization at 900 °C in air. A reversible temperature-dependent dissolution-exsolution process is observed for Au-HEO. Further correlation with distinct CO oxidation capabilities demonstrates the potential to utilize entropy effect to access self-regenerative catalysts for catalytic reactions.

Supported noble metal catalysts are critical for the treatment of air pollutants such as carbon monoxide, nitrogen oxides, hydrocarbons, etc.¹ While size control and interface engineering afford noble metal catalysts with enhanced activity and selectivity for diverse catalytic reactions, stabilizing the active species under operating conditions remains challenging.^{2–4} One of the most widely encountered problems is the unsatisfactory thermal stability of the supported noble metal catalysts. For example, operation at 800–900 °C for automobile emission control typically leads to surface migration and agglomeration of the supported noble metal catalysts.^{5–7} Dramatically decreased surface area accompanied by fewer active sites consequently result in catalyst deactivation with deteriorated performance.^{8,9} Regarding this, Nishihata *et al.*

first put forward the concept of self-regenerative catalysts, where active noble metal species move inside (as lattice cations) and outside (as supported particles) of the perovskite substrates at oxidative and reductive atmospheres, respectively.¹⁰ Since then, enormous efforts have been made to expand the self-regeneration idea,^{11–14} yet supports beyond perovskite oxides that enable ideal thermal stability for high-temperature (>600 °C) treatments have been rarely reported. In addition, most studies have focused on the enthalpy aspect of supported noble metal nanoparticles, such as charge transfer interactions and energy barrier of forming interfacial bonds,^{15,16} while other types of driving forces remain relatively unexploited.

Recent studies have indicated that entropy plays a non-negligible role in determining the structure-property relationships of multicomponent solid solutions.^{17,18} High-entropy oxides (HEOs) are a class of single-phase compounds comprised of five or more metal oxide components with random occupancy, where high configurational entropy promotes stability of the system by lowering the overall free energy.¹⁹ According to the Gibbs free energy equation ($\Delta G = \Delta H - T\Delta S$, where ΔG is the Gibbs free energy change, ΔH is enthalpy change, T is temperature, and ΔS is entropy change), HEOs tend to stabilize foreign atoms with pronounced entropy effect at a sufficiently high temperature, as observed in the cases of B, C and N doping the high-entropy alloys (HEAs).²⁰ It is thus recognized that phase stability is mainly determined by the competition between enthalpy and entropy effects that are temperature- and composition-dependent.²¹ Higher temperatures with increased compositional complexity would decrease the overall free energy, which, from a fundamental perspective, can be extrapolated to solving the aggregation issue of supported noble metals. To testify this hypothesis, we herein apply the MgO-NiO-ZnO-CuO-CoO HEOs to support 1 wt% of noble metal species including Au, Pd and Ru, and monitor their stabilization with HEOs in air at different temperatures. Interestingly, a reversible temperature-

^a Department of Chemistry, The University of Tennessee, Knoxville, Tennessee 37996, USA. E-mail: dais@ornl.gov.

^b Chemical Sciences Division, Oak Ridge National Laboratory, Oak Ridge, Tennessee 37831, USA. E-mail: suny@ornl.gov.

^c Center for Functional Nanomaterials, Brookhaven National Laboratory, Upton, New York 11973, USA

^d Department of Materials Science and Engineering, The University of Tennessee, Knoxville, Tennessee 37996, USA

^e Department of Physics and Astronomy, The University of Tennessee, Knoxville, Tennessee 37996, USA

^f Materials Science and Technology Division, Oak Ridge National Laboratory, Oak Ridge, Tennessee 37831, USA

[†] Current Address: Eyring Materials Center, Arizona State University, Tempe, Arizona 85287, USA

Electronic Supplementary Information (ESI) available: [details of any supplementary information available should be included here]. See DOI: 10.1039/x0xx00000x

dependent dissolution-exsolution process is observed for Au-HEO. This prototype of "intelligent" behavior demonstrates the

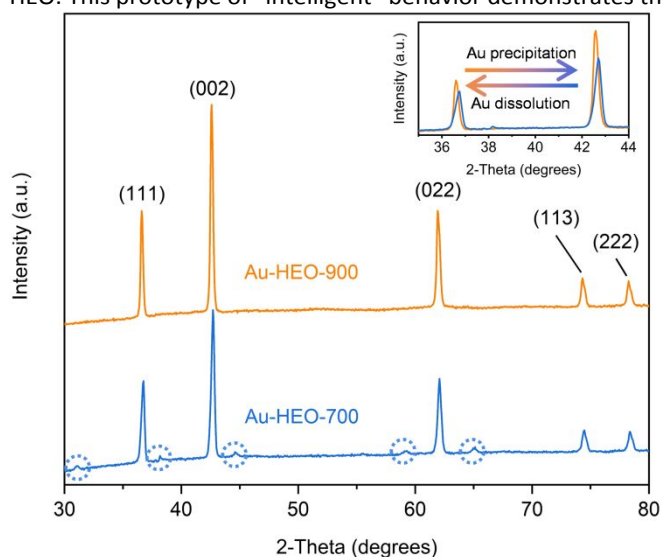


Fig. 1 Powder XRD patterns of single-phase Au-HEO-900 (orange) and multi-phase Au-HEO-700 (blue) with impurity peaks highlighted by the dotted blue circles. The inset shows the (111) and (002) diffraction peaks of Au-HEO-700 shift towards higher angles relative to those of Au-HEO-900.

potential to modulate the interplay between supported noble metal catalysts and underlying substrates by manipulating the entropy effect, which points out a novel route to accessing self-regenerative catalysts.

The noble metal-HEO samples were synthesized via a solid-state reaction with the precursors of five equal-molar transition metal oxides including MgO, CoO, NiO, CuO and ZnO, as well as 1 wt% of the noble metal oxides (Au_2O_3 , PdO, or RuO_2).¹⁹ As shown by the powder X-ray diffraction patterns (XRD) in Fig. 1 and Fig. S1, a single-phase rock-salt structure exhibiting (111), (002), (022), (113) and (222) diffraction peaks was formed upon annealing at 900 °C in air for 4 h (denoted as Au-HEO-900). Despite the difference in crystal structure, cation size and electronic charge of Au_2O_3 relative to the other metal oxide precursors (Fig. S2), absence of additional diffraction peaks and stoichiometric Au content quantified by inductively coupled plasma mass spectrometry (ICP-MS) suggest that 1 wt% of Au is well dispersed within the HEO matrix (Table S1). Rietveld refinement of the synchrotron X-ray diffraction data with GSASII reveals more details of the atomic structure of different samples (Figs. S3 and S4, and Table S2). The as-prepared HEO sample is mainly composed of the face centered cubic (FCC) phase and a small portion of the tenorite phase, which may be caused by the powder processing procedure. The Au-HEO-900 sample exhibits a pure FCC phase indicating that all the Au atoms merge into the HEO lattice. Incorporation of Au that possesses a larger radius than the transition metal atoms in the HEOs leads to a noticeable lattice expansion from 4.208 Å (HEOs) to 4.219 Å (Au-HEO-900). In contrast, no lattice compression or expansion was observed when comparing the XRD patterns of bare HEO samples annealed at 900 °C and 700 °C, respectively (Fig. S1a), implying that incorporation of Au atoms instead of the temperature-dependent transformation of

the underlying HEO support accounts for the lattice change of the FCC structure.

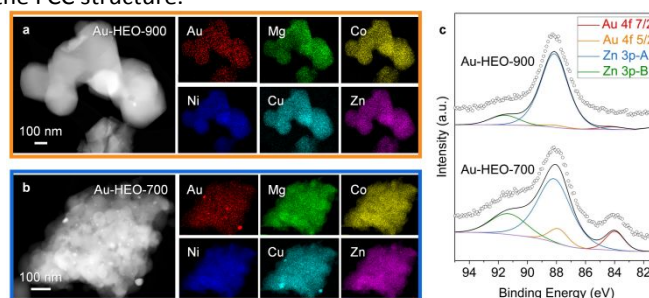


Fig. 2 HAADF-STEM images with STEM-EDS element maps of (a) Au-HEO-900 and (b) Au-HEO-700. (c) Au 4f and Zn 3p XPS spectra of Au-HEO-900 and Au-HEO-700, showing the Au amount on the HEO surface is substantially decreased after calcination in air at 900 °C.

Control experiments were performed to investigate the stabilization of Au on oxide supports with different compositions and at different temperatures. Phase separation was observed when replacing the quinary HEOs with binary (NiMgO_x) and ternary oxides (NiMgZnO_x , Fig. S5), suggesting the entropy contributions that are directly correlated with the number of oxide species play important roles in stabilizing Au. In addition, annealing Au-HEO-900 at a lower temperature (700 °C, denoted as Au-HEO-700) in air induces structure decomposition from a single-phase to multiphase state, as evidenced by the appearance of the impurity diffraction peaks (Fig. 1). With the enthalpy effect dominating over the entropy contribution at 700 °C, transition metals as Zn and Cu with higher tendencies to form non-rock-salt structures overcome the energy barrier and undergo phase separation from multicomponent, homogeneous HEOs to precipitated single-phase oxides (Fig. S2).²² Meanwhile, due to the decreased entropy contributions, Au atoms diffuse out of the rock-salt lattice which causes lattice compression as monitored by the shift of diffraction peaks towards higher angles (inset of Fig. 1). These control experiments modifying temperature or composition of the oxide support suggest that stabilization of Au into the HEO lattice is strongly correlated with the configurational entropy of the system, where a decrease in temperature or entropy would increase the overall free energy and result in destruction of the homogeneous single phase. We also observed a temperature-dependent stabilization behavior for 1 wt% Pd and Ru supported on the HEOs (Fig. S1 and Table S1). Typically, Pd and Ru tend to become oxidized at elevated temperatures in air,^{23,24} while Au remain stable due to the intrinsic inertness.²⁵ The results that all of them become well dispersed on HEOs at 900 °C demonstrate the wide applicability of exploiting the entropy effect to manipulate formation and transformation of supported noble metal species with different characteristics.

To further probe stabilization and destabilization of Au supported with HEOs, multiple characterization techniques were employed to compare the structures and compositions of Au-HEO-900 and Au-HEO-700. Fig. 2a shows the high-angle annular dark-field scanning transmission electron microscopy (HAADF-STEM) images with energy dispersive X-ray spectroscopy (EDS) element maps of Au-HEO-900, where Au as

well as Mg, Co, Ni, Cu and Zn from HEOs are uniformly distributed throughout the sample. Upon annealing at 700 °C, compositional and structural uniformity is compromised by the formation of small (7.9 ± 1.8 nm) and large (30.4 ± 7.6 nm) particles (Fig. 2b and S6). The bimodal size distribution of the emerged nanoparticles is indicative of surface migration and coalescence of the exsolved noble metal particles,²⁶ which implies that weakening of the entropy effect results in preferential exposure and aggregation of Au atoms on the surface rather than lattice stabilization within the HEOs. Besides the single Au signal on the exsolved Au particles, overlap of the Au and Cu EDS signals on some of the exsolved particles in Au-HEO-700 suggests that the exsolved Au species may react with the Cu impurities during the annealing process and ultimately form the Au-core/CuO-shell structures (Fig. S7).²⁷ Cu is distinct from the other transition metals in the HEO due to the anomalies originated from size-related effects and Jahn-Teller distortion.¹⁸ X-ray photoelectron spectroscopy (XPS), which is sensitive to the chemical environment on the surface, further verifies the temperature-dependent diffusion-precipitation behavior of Au species supported on HEOs. As shown in Fig. 2c, Au-HEO-700 exhibits characteristic Au 4f_{7/2} and Au 4f_{5/2} peaks at 84.0 and 88.0 eV, respectively.²⁸ In contrast, the intensities of both peaks are measurably decreased below the XPS detection limit for Au-HEO-900, suggesting Au atoms diffuse from the surface to the interior lattice of the HEOs.

Temperature-dependent XRD measurements were carried out to test the reversibility of the enantiotropic transformations between the single phase and multiphase state, which is a basic requirement for entropy-driven transitions.¹⁹ Starting with Au-HEO-900, the annealing temperature was switched between 700 °C and 900 °C for two cycles in air with a heating rate of 10 °C/min, and the corresponding XRD patterns during the equilibrium stage (2h at 700 °C and 4h at 900 °C) were in-situ monitored. As shown in Fig. 3a, temperature-dependent phase transitions are accompanied by the appearance and disappearance of the minor diffraction peaks from transition metal oxides and Au (Fig. S8), as well as diffraction peak shifts that are indicative of compression and expansion of the HEO lattice during Au exsolution and dissolution processes, respectively. The in-situ X-ray diffraction intensity map of the first cycle of annealing is presented in Fig. 3b, where lattice expansion of the HEO due to Au incorporation is captured by translation of the (111) and (002) diffraction peaks of the HEO structure towards lower angles during the heating process. Moreover, the two diffraction peaks from CuO and CoO (or ZnO) disappear during the heating up process, while the other one derived from Au (111) sustains longer after the temperature reaches 900 °C. Different diffusion kinetics can be attributed to the two individual processes: formation and decomposition of the HEO phase, as well as Au incorporation into and precipitation out of the HEO lattice. While it is difficult to decouple the two processes, the result is the same: driven by the competition between enthalpy and entropy effect, Au is reversibly dissolved into and exsolved out of the HEO lattice at 900 °C and 700 °C, respectively. This temperature-dependent reversible behavior also suggests that utilizing HEOs as supports may facilitate catalyst regeneration.

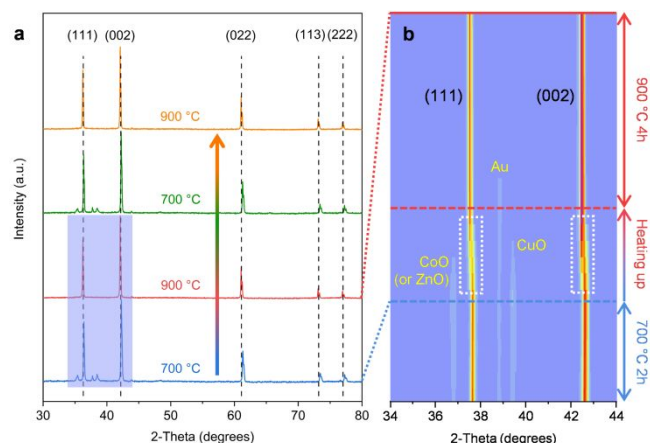


Fig. 3 (a) Temperature-dependent XRD patterns showing two annealing cycles between Au-HEO-700 and Au-HEO-900. (b) In situ X-ray diffraction intensity map as a function of 2-theta and temperature, covering the first cycle between Au-HEO-700 and Au-HEO-900, as highlighted by the light purple area in (a). Impurity diffraction peaks are attributed to CoO (or ZnO), Au and CuO through comparison with the simulated diffraction patterns (Fig. S8). The heating rate is set as 10 °C/min. Translations of the (111) and (002) diffraction peaks of the HEO towards lower angles during the heating process are highlighted by white dotted boxes.

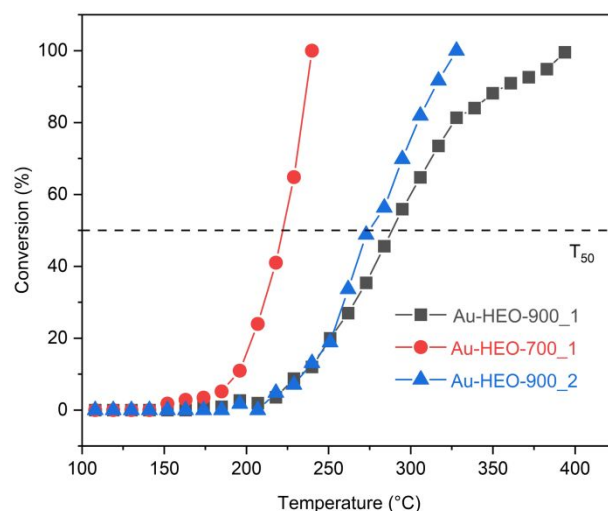


Fig. 4 CO oxidation light-off curves of the same Au-HEO-900 samples treated at 700 and 900 °C, respectively, measured with 40 mg catalysts in 1% CO balanced with dry air at a flow rate of 12 mL min⁻¹. The as-synthesized sample is noted as Au-HEO-900_1, and the one after the consecutive treatments at 700 and 900 °C is marked as Au-HEO-900_2.

CO oxidation was performed to evaluate the catalytic properties of the self-regenerative Au-HEO catalysts. As shown in Fig. 4, the as-obtained Au-HEO-900 sample delivers a lower catalytic activity ($T_{50} = 284$ °C) compared with that of Au-HEO-700 ($T_{50} = 218$ °C). Dissolution of the Au species into the HEO lattice during the formation of the single-phase Au-HEO-900 dramatically decreases the number of the active sites for CO conversion, which is also verified by the lower Au signal of Au-HEO-900 relative to that of Au-HEO-700 in the XPS spectra (Fig. 2c). Moreover, the activity of Au-HEO-900_2 ($T_{50} = 274$ °C) is close to that of Au-HEO-900_1. This demonstrates the entropy-induced dissolution and precipitation of the Au species into and out of the HEO lattice is reversible, and can be further correlated to the catalytic behaviors.

In summary, we have demonstrated that entropy effect can be exploited to access HEO-supported 1 wt% noble metal

catalysts including Au, Pd, and Ru, with the self-generation functionality and potentially enhanced anti-sintering capability. In particular, we discovered that Au remain well-dispersed within HEOs at higher temperatures with enlarged entropy contribution, while precipitate out on the surface of the oxide support at lower temperatures when enthalpy effect takes control. The structural alternations were further correlated with the CO oxidation activities, where the exposure of more active sites in Au-HEO-700 results in a higher activity compared with that of Au-HEO-900. Our study presents a fundamentally distinct pathway towards solving the sintering issue of supported noble metal catalysts at elevated temperatures. Entropy-driven stabilization of supported noble metal catalysts can be more advantageous at even higher operation temperatures, while how to expose stabilized active species on a robust support with an appreciable surface area becomes another challenging topic.²⁹ More high entropy systems including metal alloys,³⁰ oxide perovskites,³¹ carbides,³² nitrides,³³ and fluorides,³⁴ are awaiting to be explored for diverse catalytic reactions, where synergistic interactions between noble metals and high-entropy substrates determine the activity, selectivity and stability.

Conflicts of interest

There are no conflicts to declare.

Acknowledgement

This research was supported by U.S. Department of Energy, Office of Science, Office of Basic Energy Sciences, Chemical Sciences, Geosciences, and Biosciences Division, Catalysis Science program. This research used resources of the Center for Functional Nanomaterials, which is a U.S. DOE Office of Science Facility, at Brookhaven National Laboratory under Contract No. DE-SC0012704. The high-energy X-ray diffraction work by H.W., W.D. and T.E. was supported by the U.S. Department of Energy, Office of Science, Basic Energy Sciences, Materials Sciences and Engineering Division. This research also used resources of the Advanced Photon Source, a U.S. Department of Energy (DOE) Office of Science User Facility operated for the DOE Office of Science by Argonne National Laboratory under Contract No. DE-AC02-06CH11357. We thank Douglas Robinson for the assistance in the synchrotron X-ray experiment, and Harry M. Meyer III for XPS acquisition and analysis.

- P. Munnik, P. E. de Jongh and K. P. de Jong, *Chem. Rev.*, 2015, **115**, 6687–6718.
- A. T. Bell, *Science*, 2003, **299**, 1688–1691.
- M. Cargnello, *Chem. Mater.*, 2019, **31**, 576–596.
- T. W. Hansen, A. T. DeLaRiva, S. R. Challa and A. K. Datye, *Acc. Chem. Res.*, 2013, **46**, 1720–1730.
- J. T. Kummer, *J. Phys. Chem.*, 1986, **90**, 4747–4752.
- J. Jones, H. Xiong, A. T. DeLaRiva, E. J. Peterson, H. Pham, S. R. Challa, G. Qi, S. Oh, M. H. Wiebenga, X. I. Pereira Hernandez, Y. Wang and A. K. Datye, *Science*, 2016, **353**, 150–154.
- H. Chen, W. Lin, Z. Zhang, K. Jie, D. R. Mullins, X. Sang, S.-Z. Yang, C. J. Jafta, C. A. Bridges, X. Hu, R. R. Unocic, F. Jie, P. Zhang and S. Dai, *ACS Mater. Lett.*, 2019, **1**, 83–88.
- H. Chen, J. Fu, P. Zhang, H. Peng, C. W. Abney, K. Jie, X. Liu, M. Chi and S. Dai, *J. Mater. Chem. A*, 2018, **6**, 11129–11133.
- C. H. Bartholomew, *Appl. Catal. A Gen.*, 2001, **212**, 17–60.
- Y. Nishihata, J. Mizuki, T. Akao, H. Tanaka, M. Uenishi, M. Kimura, T. Okamoto and N. Hamada, *Nature*, 2002, **418**, 164–167.
- H. Tanaka, M. Uenishi, M. Taniguchi, I. Tan, K. Narita, M. Kimura, K. Kaneko, Y. Nishihata and J. Mizuki, *Catal. Today*, 2006, **117**, 321–328.
- H. Tanaka, M. Taniguchi, M. Uenishi, N. Kajita, I. Tan, Y. Nishihata, J. Mizuki, K. Narita, M. Kimura, K. Kaneko, *Angew. Chem. Int. Ed.*, 2006, **45**, 5998–6002.
- T. M. Onn, M. Monai, S. Dai, E. Fonda, T. Montini, X. Pan, G. W. Graham, P. Fornasiero and R. J. Gorte, *J. Am. Chem. Soc.*, 2018, **140**, 4841–4848.
- M. B. Katz, G. W. Graham, Y. Duan, H. Liu, C. Adamo, D. G. Schlom and X. Pan, *J. Am. Chem. Soc.*, 2011, **133**, 18090–18093.
- C. T. Campbell, *Acc. Chem. Res.*, 2013, **46**, 1712–1719.
- S. Dai, *ChemSusChem*, 2020, **13**, 1915–1917.
- J.-W. Yeh, S.-K. Chen, S.-J. Lin, J.-Y. Gan, T.-S. Chin, T.-T. Shun, C.-H. Tsau and S.-Y. Chang, *Adv. Eng. Mater.*, 2004, **6**, 299–303.
- C. Oses, C. Toher and S. Curtarolo, *Nat. Rev. Mater.*, 2020, **5**, 295–309.
- C. M. Rost, E. Sachet, T. Borman, A. Moballegh, E. C. Dickey, D. Hou, J. L. Jones, S. Curtarolo and J.-P. Maria, *Nat. Commun.*, 2015, **6**, 8485.
- M.-H. Tsai and J.-W. Yeh, *Mater. Res. Lett.*, 2014, **2**, 107–123.
- D. Miracle, J. Miller, O. Senkov, C. Woodward, M. Uchic and J. Tiley, *Entropy*, 2014, **16**, 494–525.
- A. Sarkar, R. Djenadic, N. J. Usharani, K. P. Sanghvi, V. S. K. Chakravadhanula, A. S. Gandhi, H. Hahn and S. S. Bhattacharya, *J. Eur. Ceram. Soc.*, 2017, **37**, 747–754.
- C. Carrillo, T. R. Johns, H. Xiong, A. DeLaRiva, S. R. Challa, R. S. Goeke, K. Artyushkova, W. Li, C. H. Kim and A. K. Datye, *J. Phys. Chem. Lett.*, 2014, **5**, 2089–2093.
- H. Over and A. P. Seitsonen, *Science*, 2002, **297**, 2003–2005.
- L. K. Ono and B. Roldan Cuenya, *J. Phys. Chem. C*, 2008, **112**, 4676–4686.
- Y. Sun, Y. Wang, J. Y. C. Chen, K. Fujisawa, C. F. Holder, J. T. Miller, V. H. Crespi, M. Terrones and R. E. Schaak, *Nat. Chem.*, 2020, **12**, 284–293.
- W. Zhan, J. Wang, H. Wang, J. Zhang, X. Liu, P. Zhang, M. Chi, Y. Guo, Y. Guo, G. Lu, S. Sun, S. Dai and H. Zhu, *J. Am. Chem. Soc.*, 2017, **139**, 8846–8854.
- M. P. Casaletto, A. Longo, A. Martorana, A. Prestianni and A. M. Venezia, *Surf. Interface Anal.*, 2006, **38**, 215–218.
- X. Mao, A. C. Foucher, T. Montini, E. A. Stach, P. Fornasiero and R. J. Gorte, *J. Am. Chem. Soc.*, 2020, **142**, 10373–10382.
- Y. Yao, Z. Huang, P. Xie, S. D. Lacey, R. J. Jacob, H. Xie, F. Chen, A. Nie, T. Pu, M. Rehwoldt, D. Yu, M. R. Zachariah, C. Wang, R. Shahbazian-Yassar, J. Li and L. Hu, *Science*, 2018, **359**, 1489–1494.
- S. Jiang, T. Hu, J. Gild, N. Zhou, J. Nie, M. Qin, T. Harrington, K. Vecchio and J. Luo, *Scr. Mater.*, 2018, **142**, 116–120.
- P. Sarker, T. Harrington, C. Toher, C. Oses, M. Samiee, J.-P. Maria, D. W. Brenner, K. S. Vecchio and S. Curtarolo, *Nat. Commun.*, 2018, **9**, 4980.
- T. Jin, X. Sang, R. R. Unocic, R. T. Kinch, X. Liu, J. Hu, H. Liu and S. Dai, *Adv. Mater.*, 2018, **30**, 1707512.
- T. Wang, H. Chen, Z. Yang, J. Liang and S. Dai, *J. Am. Chem. Soc.*, 2020, **142**, 4550–4554.

